

## IMAGE FUSION WAVELET-BASED SHARPNESS ENHANCEMENT OF LROC WIDE ANGLE CAMERA IMAGES – PERFORMANCE COMPARISON AMONG WAVELET TYPES

A. Awumah, P. Mahanti, M. S. Robinson, H. Sato. School of Earth and Space Exploration, Arizona State University, 1100 S. Cady Mall, Interdisciplinary A, Tempe, AZ, 85287-3603; (aawumah@ser.asu.edu)

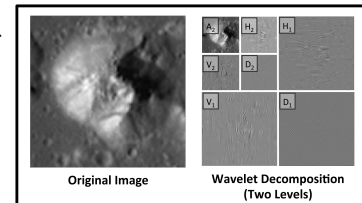
**Introduction:** Image fusion involves integrating elements from two or more characteristically different, multi-sensor, and/or multi-temporal images to create a new image that relays more information than the component images provide. In Earth-based remote sensing, image fusion is employed to enhance the spatial resolution of a multi-spectral (MS) image by integrating the MS spectral content with geometric (edge) details from a higher-resolution panchromatic (Pan) image. The derived high-resolution multispectral (HRMS) image can then be said to have both high-spectral (from the original MS) and high-spatial (from the Pan) resolutions. Although widely utilized in Earth-based remote sensing, image fusion as applied to planetary images is still relatively uncommon; a few known applications include its use in Viking Orbiter images of Mars [1,2] and Chandrayaan and SELENE images of the Moon [3].

In the current design of most remote sensing imaging systems, an inherent trade-off exists between a system's ability to highly resolve spatial and spectral information, due to the standing inverse relationship between the system's instantaneous field-of-view and spectral bandwidth sizes. Additionally, planetary mission payload mass restrictions, and data transmission and cost limitations make the integration of an on-board HRMS imaging system typically unfeasible. Thus, planetary missions which integrate both low-resolution MS and high-resolution Pan instruments stand to benefit from image fusion as a suitable post processing solution for sharpness enhancement of MS images.

Several standard image fusion methods have been developed which establish various means of extracting geometric details from the Pan and injecting it into the MS. While many of these methods are successful at enhancing the spatial resolution of the MS, results may contain significant color distortion. In a previous work, the following six well-known image fusion methods were applied to Lunar Reconnaissance Orbiter Camera (LROC) Narrow Angle Camera (NAC) and Wide Angle Camera (WAC) images: Intensity-Hue-Saturation, Brovey Transform, Principal Component Analysis, the University of New Brunswick method, High Pass Filter and Additive Wavelet [4]. In both qualitative (via visual inspection) and quantitative (metric-based) assessments in which spectral content preservation was emphasized over sharpness enhancement, the wavelet-based image fusion method

yielded the best spectral performance. In this study we apply different wavelet-based image fusion methods to lunar images from the LROC WAC and NAC system based on wavelet family and level of decomposition, and assess results for overall spatial and spectral quality.

**Figure 1.** Two levels of wavelet decomposition applied to a WAC image of Copernicus Crater's central peak.



**Wavelets Overview:** The wavelet-based method utilizes a wavelet transform to decompose an image in the scale-space domain into its low and high frequency components. In an image, sharpness details, like edges, are characterized by a high rate-of-change in pixel values; thus geometric details are, in the frequency domain, high-frequency information. For the purposes of sharpness enhancement of MS lunar imagery, in which the primary objective is to increase the spatial resolution of the MS image with minimal distortion to its spectral content, the wavelet-based image fusion method is particularly useful. In this method the schema by which high-frequency information from the Pan is extracted and combined with MS spectral content (lower frequency information) results in a spatially enhanced yet minimally spectrally distorted MS when compared to other standard methods [5].

In wavelet-based image fusion, the separation of image high and low frequency content is governed by a set of wavelet and scale functions (wavelet families) with specific properties [5], and the levels of decomposition implemented. The latter allows for filtering of high frequency information at successively coarser scales. In this work, each successive level of decomposition reduces the image scale by one quarter.

**Method:** Prior to image fusion, NAC left and right image pairs and WAC images are radiometrically calibrated and mosaicked utilizing USGS ISIS software [6]. WAC images consist of seven bands (two UV (321 nm and 360 nm) and five visible (415, 566, 604, 643, 689 nm)) [7]. The NAC spectral response range is 400 to 760 nm [8]. Pixel scales used for the fusion process are 64 meters (m) and 256 m for the WAC visible and UV bands, respectively.

Due to the scale difference, visible and ultra-violet bands are treated as separate MS datasets and thus HRMS products are created for both (HRMS-Vis and HRMS-UV). NAC images are resampled from the native 0.5 to 1.5 m scale to satisfy the target Pan-to-MS scale ratio of 1:4.

The wavelet families tested were Haar (db 1), Daubechies four and six (db 4 & 6), and Symlets two, four, and six (Sym 2, 4, & 6). Each wavelet family provides a set of functions used to decompose Pan (NAC) and MS (WAC) images at designated levels of decomposition. In this work, levels one through four are tested. After a wavelet transformation, decomposed Pan and MS images are described by horizontal (H), vertical (V), and diagonal (D) detail (higher frequency, edge) coefficients and an approximation (A) coefficient (lower frequency information; Fig. 1). For image fusion at one level of decomposition, H, V, and D detail coefficients of the Pan image replace the corresponding detail coefficients of the MS; a reverse wavelet transform is then applied to the combined Pan and MS components. The newly transformed image is added to the MS to yield the HRMS image. For image fusion at two levels of decomposition, each image's first-level A coefficient is further decomposed into another set of (coarser) approximation and detail coefficients (Fig. 1). The Pan second-level detail coefficients and MS second-level A coefficient are reverse-transformed into a new, synthesized level-one approximation coefficient. The Pan level-one detail coefficients and the synthesized A coefficient are reverse-transformed to retrieve an HRMS which has incorporated more high-frequency detail with the additional level of filtering. Three and four levels of decomposition follow the same process with additional filtering occurring at even coarser scales. All image fusion algorithms are written and executed in MATLAB.

**Results:** The image fusion methods described above were applied to LROC observations of Brayley Crater (NAC M1145042491 (left and right pair) and WAC M135432702C). Three image fusion quality metrics assessed the spatial and spectral quality of the HRMS product: the Average Gradient (AG), the Relative Dimensionless Global Error in Synthesis (French acronym, ERGAS), and Universal Image Quality Index (UIQI) [9,10,11]. A larger AG suggests a higher spatial resolution, while an ERGAS value of zero indicates total spectral content preservation. UIQI assesses overall quality of fusion based on a loss of correlation between the HRMS and original images, radiometric distortion, and contrast distortion; a UIQI equal to one indicates zero spectral distortion.

The Haar (db 1) wavelets, with four level of

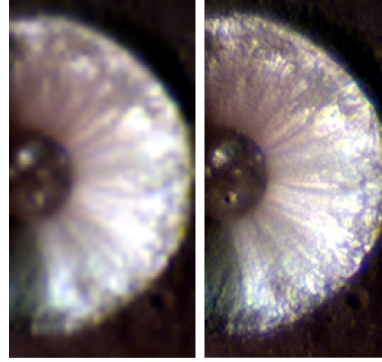


**Figure 2.** Left: MS (before image fusion) composite image of Brayley Crater. Right: HRMS-Vis (after d6, one level wavelet fusion) composite image. Red, green, and blue bands are 689, 415, & 321 nm.

	Haar (db1)				db 4				db 6			
	lev 1	lev 2	lev 3	lev 4	lev 1	lev 2	lev 3	lev 4	lev 1	lev 2	lev 3	lev 4
AG	0.01832	0.01958	0.02052	0.02080	0.01811	0.01872	0.01898	0.01912	0.01809	0.01869	0.01939	0.02013
ERGAS	2.32556	2.77990	3.13785	3.38136	2.22168	2.51375	2.76174	3.00296	2.21064	2.50037	2.86175	3.20570
UIQI	0.99978	0.99955	0.99927	0.99901	0.99982	0.99970	0.99956	0.99939	0.99982	0.99971	0.99949	0.99920

	Sym 2				Sym 4				Sym 6			
	lev 1	lev 2	lev 3	lev 4	lev 1	lev 2	lev 3	lev 4	lev 1	lev 2	lev 3	lev 4
AG	0.01817	0.01882	0.01955	0.01975	0.01811	0.01872	0.01900	0.01917	0.01809	0.01869	0.01938	0.02013
ERGAS	2.25567	2.54957	2.91248	3.14635	2.22100	2.51361	2.75354	3.00627	2.21106	2.49892	2.85756	3.20624
UIQI	0.99980	0.99968	0.99946	0.99926	0.99982	0.99970	0.99957	0.99939	0.99982	0.99971	0.99950	0.99920

**Table 1.** Spatial and spectral quality test results

decomposition, yielded the largest average gradient result for HRMS-Vis, providing the best spatial performance; it also yielded the poorest spectral test results as indicated by its ERGAS and UIQI values (Tab. 1). Db 6, at one level of decomposition, yielded the least spatially enhanced HRMS, yet performed the best spectrally (Fig 2). The spatial and spectral test results highlight the relationship between increasing the spatial resolution of an MS and increasing its spectral distortion during the fusion process; the wavelet family and levels of decomposition combination that performed the best spatially also performed the worst spectrally.

**References:** [1] B.A. Archinal, et al. (2004) *Intl. Arch. of Photog. and Rem. Sens.* 35:B4. [2] M.S. Robinson (1994) *Astronomy* 22:30. [3] A. Lavanya, et al. (2011) in *Recent Trends in Information Technology (ICRTIT), 2011 International Conference on* 920–925 IEEE. [4] P. Mahanti, et al. (2016) *ISPRS-International Archives of the Photogrammetry, Remote Sensing and Spatial Information Sciences* 685–692. [5] K. Amolins, et al. (2007) *ISPRS Journal of Photogrammetry and Remote Sensing* 62(4):249. [6] J. Anderson, et al. (2004) in *Lunar and Planetary Science Conference* vol. 35. [7] P. Mahanti, et al. (2015) *Space Sci. Revs.* 1–38. [8] D. Humm, et al. (2015) *Space Sci. Revs.* 1–43. [9] Z. Li, et al. (2005) *Pattern Recognition Letters* 26(13):2006. [10] L. Wald (2002) *Data fusion: definitions and architectures: fusion of images of different spatial resolutions* Presses des MINES. [11] B. C. A. Wang Zhou (2002) *IEEE Signal Processing Letters*, 81–84.